Photoexcitation, trapping, and recombination processes of the *F*-type centers in lasing MgO microcrystals

Y. Uenaka

Department of Chemistry, Faculty of Science, Kobe University, Nada, Kobe 657-8501, Japan

T. Uchino

Department of Chemistry, Graduate School of Science, Kobe University, Nada, Kobe 657-8501, Japan

We report results of a detailed temperature dependence of photoluminescence (PL) decay time and continuous emission properties of the *F* and *F*$^+$ centers in recently reported lasing MgO microcrystals [T. Uchino and D. Okutsu, Phys. Rev. Lett. **101**, 117401 (2008)]. Thermally induced ionization and carrier trapping play a vital role in the entire emission processes of the *F*-type centers, especially at time scales longer than microseconds. In these time scales the PL decay profiles tend to exhibit a power-law behavior over more than 3−4 decades of time, implying thermally activated hopping and tunneling of the trapped electrons. Such delayed PL signals show two maxima in intensity at temperatures of ∼130 and ∼300 K. This apparently anomalous temperature dependence is also indicative of the thermally stimulated emission processes of the originally photoexcited *F* and *F*$^+$ centers. The PL spectra above lasing threshold exhibit temperature-dependent broadening, demonstrating that the thermal vibrations of the crystal lattice affect the stimulated emission scheme as well. On the basis of these experimental results, a model of the photoexcitation, trapping, and recombination processes of the *F*-type centers is presented.

I. INTRODUCTION

Magnesium oxide is one of the most thoroughly studied metal-oxide materials not only in terms of a simple oxide system with a rocksalt structure but also of structural defects.[1] Recently, structure and properties of defects in MgO have attracted renewed interest in view of their intriguing electronic states, giving rise to a variety of optical,[2–6] magnetic,[7–9] and electron-emission[10–14] properties. These renewed findings have revealed that our knowledge about defects in MgO is still incomplete, hence requiring further investigations on their structural and electronic properties.

It has been well recognized that MgO has several types of intrinsic defects or color centers, including oxygen and magnesium vacancies. Among other color centers, neutral oxygen vacancies (*F* centers) and positively charged oxygen vacancies (*F*$^+$ centers) have been extensively investigated during the past decades.[15–21] The *F* and *F*$^+$ centers exhibit broad photoluminescence (PL) bands peaking at ∼2.3 eV (∼500 nm) and ∼3.2 eV (∼400 nm), respectively, whereas the optical absorption of both types of centers is peaked essentially at the same energy of ∼5 eV (∼250 nm). In general, these *F*-type centers have been incorporated into MgO by the following two methods.[15] One is by irradiation with energetic particles, such as neutrons, electrons, and ions. The other method is by thermochemical reduction performed under highly reducing conditions at temperatures ≳ 2000 K, leading to stoichiometric deficiency in the oxygen sublattice. According to the previous investigations,[17,18] the MgO crystals thus prepared often include a perceptible amount of extrinsic impurities, e.g., hydride ions (*H*$^-$) and metal-based impurities, which potentially perturb the electronic states of the intrinsic *F*-type centers. It has also been demonstrated that these impurity-related defects behave as electron and/or

hole trapping centers, resulting in a long-lived (∼10^3 s) PL decay time of the *F*-type centers and even the *F*$^+$-to-*F* photoconversion.[19,20]

Recently, we[5,6] have proposed a simple but effective method to introduce *F*-type centers into MgO as an alternative to conventional irradiation and thermochemical reduction methods. The proposed method utilizes the solid phase reaction between silicon monoxide (SiO) and Mg. When the Mg/SiO mixture of molar ratio 2:1 is heated under Ar atmosphere at 450 °C, substoichiometric MgO molecules are preferentially sublimated, forming colored micrometer-sized MgO crystals. The resulting MgO microcrystals show efficient PL emissions attributed to the *F* and *F*$^+$ centers. It should be worth mentioning that these colored MgO microcrystals exhibit a so-called random lasing effect,[22,23] which is induced by multiple scattering in an amplifying disordered medium, even at room temperature.[5,6]

The purpose of this work is to carry out a detailed temperature dependence study of the PL characteristics, including the emission intensity, spectral shape, and decay time, of the colored MgO microcrystals. We have found that that the observed PL features are quite different from those observed previously for the energetic particle-irradiated and thermochemically reduced MgO crystals. For example, the observed PL intensity and decay profiles do not show systematic changes with temperature, hence demonstrating an apparently anomalous temperature dependence. We also investigate the effect of temperature on the random lasing phenomena of the MgO microcrystals. On the basis of the experimental results, we will present a model of the photoexcitation, trapping, and recombination processes of the *F*-type centers in the material, especially in view of the thermally activated and assisted phenomena.

II. EXPERIMENTAL PROCEDURES

In our previous papers,[5,6] we utilized the solid phase reaction between silicon SiO and Mg to obtain colored MgO microcrystals. This method allows us to indeed obtain lasing MgO microcrystals as a result of the sublimation of MgO_x ($x < 1$) species, but the reaction between SiO and Mg is highly exothermic and sometimes occurs in an explosive manner. This leads to unavoidable contaminations arising from the reaction subproducts, such as Si and Mg_2Si,[5] which may degrade the emission properties of the colored MgO crystals. To circumvent the problem we here employed B_2O_3 instead of SiO as an oxide to react with Mg. It has previously been demonstrated that in the Mg/B_2O_3 system, the following chemical reactions occur depending on the reaction temperature:[24,25]

$$3Mg + B_2O_3 \rightarrow 2B + 3MgO (\gtrsim 500\,^{\circ}C), \tag{1}$$

$$4Mg + B_2O_3 \rightarrow MgB_2 + 3MgO (\gtrsim 700\,^{\circ}C). \tag{2}$$
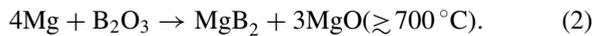
We have found that substoichiometric MgO_x ($x < 1$) molecules are also sublimated when the Mg/B_2O_3 mixture is heated at 700 °C under argon atmosphere using a stoichiometric excess amount of Mg, similar to the case of the Mg/SiO mixture. It should be worth mentioning that the reaction between Mg and B_2O_3 does not occur in an explosive way but can be well controlled. Furthermore, as will be shown below, the resulting colored MgO microcrystals hardly contain any reaction subproducts.

Pure Mg (99.9%) and B_2O_3 (99.9%) powders were used as starting materials. The Mg/B_2O_3 mixture of molar ratio of 5:1, namely, the Mg excess condition, was thoroughly mixed and put in a cylindrical alumina crucible. This crucible was located inside a larger rectangular alumina crucible, which was closed with a 4-mm-thick alumina lid. This set of crucibles was placed in an electric furnace. The furnace was evacuated down to ~30 Pa before purging with argon. The temperature of the furnace was raised to 700 °C at a rate of ~10 °C/min and kept constant at 700 °C for 2 h under flowing argon environment. After the heating process, we found that a substantial amount of white powder was deposited outside the inner crucible. We collected the thus deposited powder along with the substances found in the bottom of the inner crucible. The respective powder samples were stored in a desiccator for later characterization.

Powder x-ray diffraction (XRD) patterns of the samples were obtained with a diffractometer (Rigaku, SmartLab) using Cu $K\alpha$ radiation. Fourier transform infrared spectra (FTIR) were collected with a FTIR spectrometer (Perkin-Elmer, Spectrum 1000) in the frequency region from 400 to 4000 cm^{-1}. A conventional KBr disk technique was employed to measure the FTIR spectra with ten scans and a resolution of 1 cm^{-1}. Diffuse reflectance spectra were measured using a spectrophotometer (Hitachi, UV-3500) equipped with an integrating sphere to collect scattered light. Steady-state PL spectra and time-resolved PL signals in the millisecond-to-second time region were recorded on a spectrofluorometer (JASCO, FP 6600) by using a monochromated xenon lamp (150 W) and a mechanical shutter. Time-resolved PL measurements in the nanosecond-to-microsecond time region were also carried out with a gated image-intensified charge-coupled

device (Princeton Instruments, PI-MAX:1024RB) and a 150 lines/mm grating by using the third harmonic (355 nm) or the fourth harmonic (266 nm) of a pulsed Nd:yttrium aluminum garnet (YAG) laser (Spectra Physics, INDI 40, pulse width 8 ns, repetition rate 10 Hz) as an excitation source. During the PL measurements, the sample temperature was controlled in a closed-cycle N_2 cryostat. To induce random lasing the pump beam was loosely focused with an $f = 150$ mm lens in such a way that the beam diameter was reduced from ~10 to ~3 mm. The focused beam was irradiated onto the powders placed in a sample holder with a 1-mm-thick silica glass window. The pumping density of an incoming focused laser beam was continuously varied from 10 to 120 mJ/cm^2 with a variable laser beam attenuator (Metrolux, ML2100).

III. RESULTS

A. XRD measurements

Figure 1 shows the XRD patterns of the substances found in the bottom of the inner alumina crucible [Fig. 1(a)] and the white powder deposited outside the inner crucible [Fig. 1(b)]. The XRD pattern shown in Fig. 1(a) consists of the diffraction peaks attributed to Mg [Joint Committee on Powder Diffraction Standards (JCPDS) file, card number 35-0821], MgO (JCPDS 45-946), and MgB_2 (JCPDS 38-1369). This indicates that the solid phase reaction between Mg and B_2O_3 proceeds according to Eq. (2) and some of the unreacted Mg metal still remains in the inner crucible. On the other hand, all the diffraction peaks of the deposited powder are indexed to MgO [see Fig. 1(b)]. Hence it can safely be said that the deposited power exclusively comprises MgO particles and contains basically no reaction subproducts. As will be shown later, the deposited MgO powder exhibits optical absorption and emission bands attributed to various types of oxygen vacancies, namely, the F-type centers.

B. Infrared absorption and ultraviolet-visible diffuse reflectance spectra

As mentioned in the Introduction, previously reported colored MgO single crystals, especially those prepared by
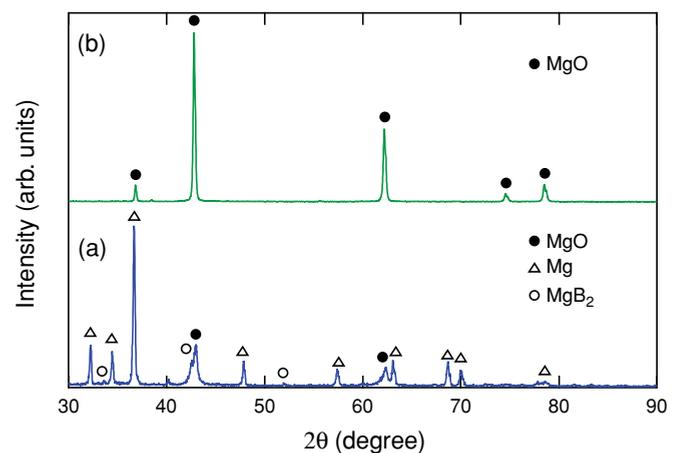
FIG. 1. (Color online) XRD patterns of (a) the materials found in the bottom of the inner alumina crucible and (b) the powders deposited outside it.
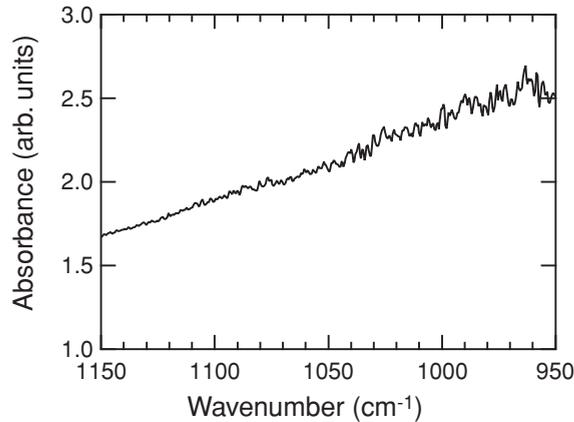
FIG. 2. A typical infrared spectrum of the deposited MgO powder obtained with a KBr disk technique.

thermochemical reduction, generally contain H^- ions as substitutional impurities.[17–20,26] The source of the hydrogen is believed to be moisture sorbed in MgO powder prior to single-crystal growth.[26] The fundamental vibrations of substitutional H^- ions occur at 1053, 1032, and 1024 cm^{-1} at 295 K.[26] Previous studies[17,18,20] have further demonstrated that the decay dynamics of the F-center emission in MgO is strongly affected by the H^- ions, which can serve as traps for excited electrons. The reported long-lived luminescence, which can last as long as 10^3 s, has been ascribed to successive trapping and detrapping of electrons by the H^- complex.[17] It is hence interesting to investigate whether or not the MgO powder obtained in this work yields the above H^--related infrared absorption bands.

We carried out a systematic infrared absorption measurement by changing the amount of the MgO powder dispersed into KBr powder. However, we did not recognize any H^--related infrared absorption bands in the wave-number region from 1000 to 1100 cm^{-1} for all the infrared spectra obtained in this work; a typical example of the infrared spectra obtained is shown in Fig. 2. This demonstrates that the present MgO powder hardly contains substitutional H^- ions in the crystal. This is also consistent with the PL decay measurements (see Sec. III D), showing the lack of a very long-lived ($\sim 10^3$ s) PL decay component in our MgO sample.

The diffuse reflectance spectra of the MgO powder in the ultraviolet (UV)-visible region are shown in Fig. 3. In this work, all the diffuse reflectance measurements were carried out at room temperature. One sees a single broad intense peak at 248 nm (5.0 eV), which is attributed to the absorption of the F and F^+ centers. According to the previous UV-visible absorption measurements on colored MgO single crystals,[19] a broad absorption band centered at 2.3 eV (540 nm) develops after continuous excitation with ~ 5.0 eV light. The 2.3-eV band is attributed to V-type centers or holes trapped at cation vacancies compensated by Al^{3+}, F^-, and OH^- impurities.[19] As shown in Fig. 3, our MgO sample does not show any change in the whole UV-visible region investigated even after UV irradiation at 5.0 eV for 30 min. Thus, it can be safely said that the present MgO powder does not virtually contain any impurity-derived V-type centers, which can potentially trap holes under continuous optical excitation of the F and F^+ centers.
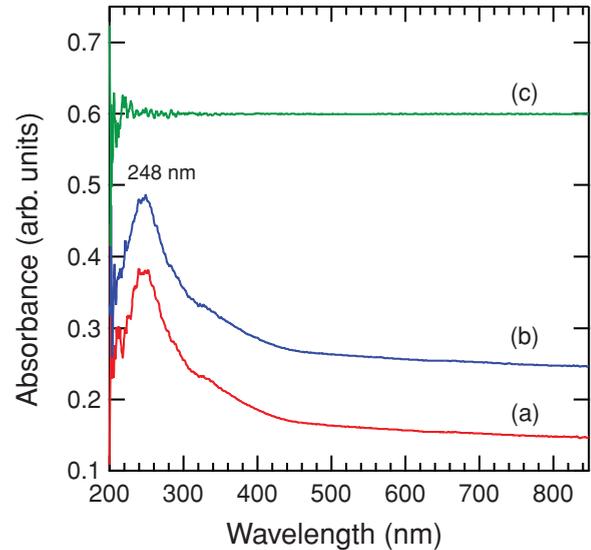
FIG. 3. (Color online) Diffuse reflectance spectra of the MgO powder in the UV-visible region: (a) the as-prepared MgO powder, (b) the MgO powder after excitation with 250-nm light for 30 min, and (c) the difference spectrum between (a) and (b).

The above infrared absorption and UV-visible diffuse reflectance measurements allow us to conclude that previously reported extrinsic impurities, such as H^-, Al^{3+}, F^-, and OH^-, hardly exist in the present MgO powder. This ensures that we do not need to take into account a possible effect of these impurities in discussing the photoexcitation and emission processes of the sample.

C. Steady-state photoluminescence spectra

Figure 4 shows the temperature dependence of the steady-state PL spectrum of the deposited MgO powder under continuous excitation of 256-nm light. One notices from Fig. 4 that the
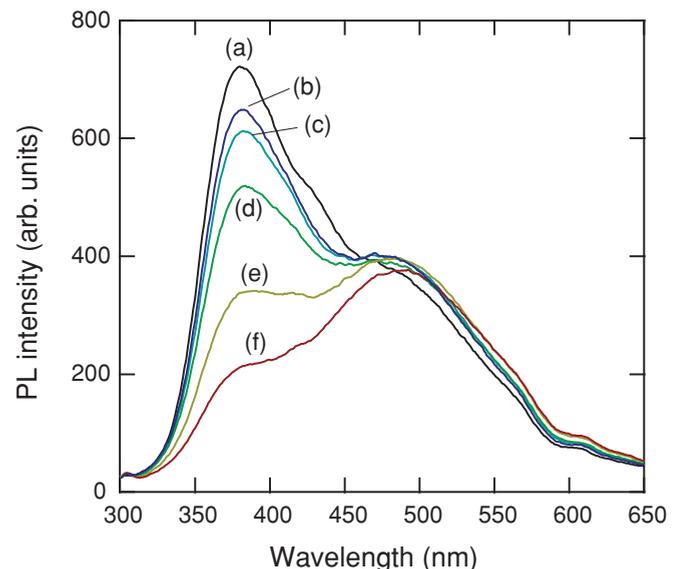
FIG. 4. (Color online) Steady-state PL spectra of the MgO powder measured at different temperatures: (a) 77, (b) 150, (c) 200, (d) 250, (e) 300, and (f) 350 K. The excitation wavelength is 256 nm.
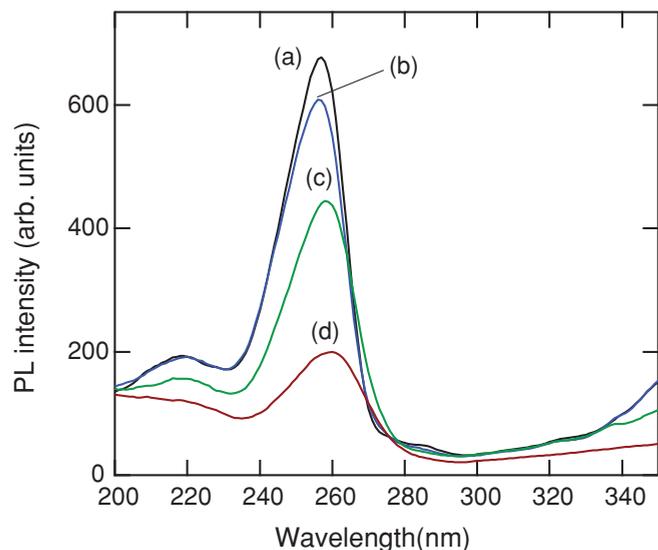
FIG. 5. (Color online) Steady-state PL excitation spectra of the F^+ center in the MgO powder measured at different temperatures: (a) 77, (b) 150, (c) 250, and (d) 350 K. The monitor wavelength is 380 nm.

MgO sample exhibits two broad PL bands peaking at 490 nm (2.5 eV) and 380 nm (3.2 eV), which are attributed to the F and F^+ luminescence bands, respectively. Figures 5 and 6 illustrate the corresponding PL excitation (PLE) spectra. The 380-nm band (the F^+-center emission) shows a decrease in intensity with increasing temperature (see Fig. 5), while the intensity of the 490-nm band (the F-center emission) does not show a systematic change with temperature (see Fig. 6). We will discuss the origin of the difference in temperature dependence between the F- and F^+-center emission bands in Sec. IV.
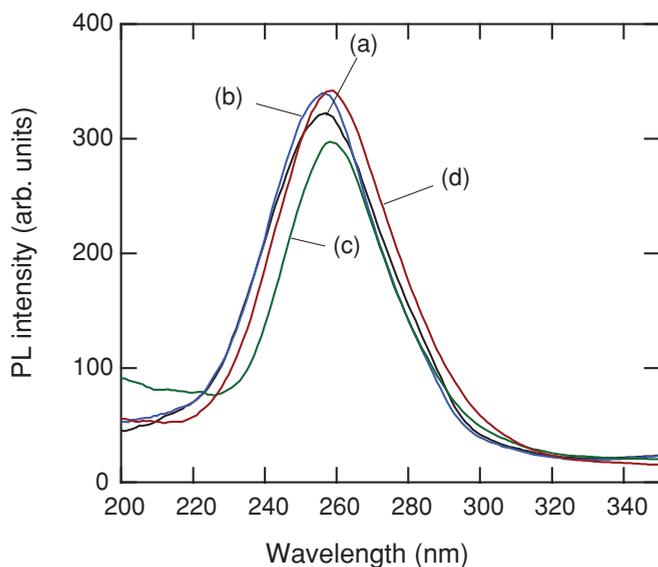
D. Time-resolved photoluminescence measurements

Previous time-resolved PL measurements of MgO crystals[27] have demonstrated that in the low hydrogen containing samples the F and F^+ luminescence bands decay together with only a minor difference, while in the high hydrogen containing samples the major trend is the switch from short-lived F^+ to long-lived F character. Thus, it is expected that the present MgO sample, in which the concentration of H$^-$ ions is negligible, show similar decay profiles for both the F- and F^+-center luminescence bands. We, however, found that this is not the case; rather, these two types of centers exhibit quite different temperature-dependent PL decay characteristics. Furthermore, we found that the decay kinetics of these F-type centers can be classified into three different time scales, namely, (1) nanosecond-to-microsecond, (2) microsecond-to-millisecond, and (3) millisecond-to-second time scales, depending on their characteristic PL behaviors. Thus, in what follows, we will present the results of time-resolved PL measurements obtained in the respective time scales.

1. Nanosecond-to-microsecond time scale

Figure 7 shows the temperature dependence of the time-integrated PL spectrum of the deposited MgO powder obtained in the 0-1 μs time window under excitation of the fourth harmonic (266 nm) of a pulsed Nd:YAG laser. The irradiation fluence was $\sim$3 mJ/cm^2, which is well below the lasing threshold ($\sim$60 mJ/cm^2) of this sample. We see from Fig. 7 that in this time window, the F^+-center PL band peaking at $\sim$390 nm, is the predominant emission center in the entire temperature range studied. Figure 7 also demonstrates a monotonic decrease in the peak intensity with increasing temperature. The semilog plot of the wavelength-integrated PL intensity versus reciprocal temperature revealed two straight lines of different

FIG. 6. (Color online) Steady-state PL excitation spectra of the F center in the MgO powder measured at different temperatures: (a) 77, (b) 150, (c) 250, and (d) 350 K. The monitor wavelength is 490 nm.
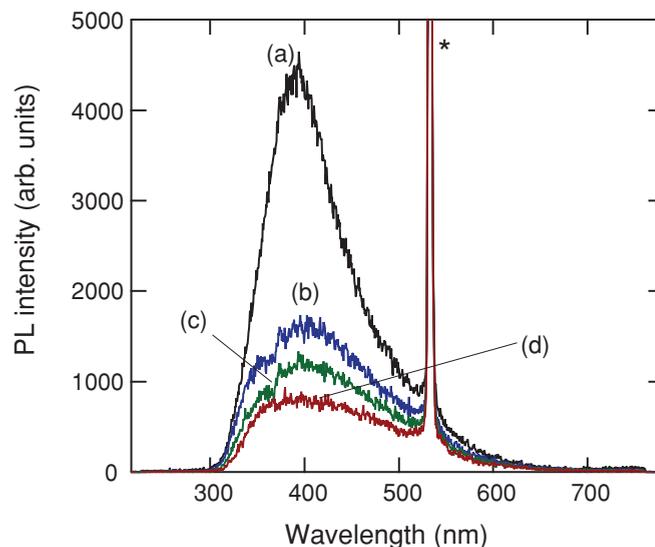
FIG. 7. (Color online) Time-integrated (0–1 μs) PL spectra of the deposited MgO powder under excitation of the fourth harmonic (266 nm) of a pulsed Nd:YAG laser measured at different temperatures: (a) 77, (b) 150, (c) 250, and (d) 350 K. The irradiation fluence was $\sim$3 mJ/cm^2. The asterisk indicates the second harmonic (532 nm) of the Nd:YAG laser contaminated in the incident beam.
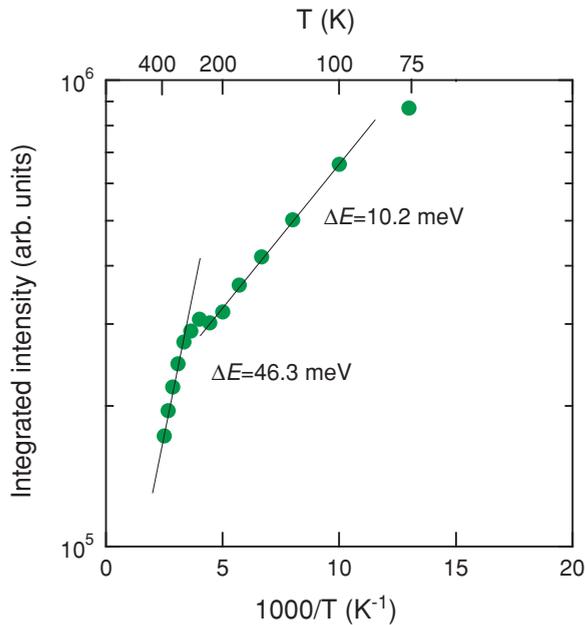
FIG. 8. (Color online) Spectrally integrated intensity of the PL spectra shown in Fig. 7 as a function of $1/T$. The apparent thermal activation energies obtained from a linear fit to the data in the in the lower ($100-200$ K) and higher ($300-400$ K) temperature regions are also shown.

slopes (see Fig. 8). This suggests that there exist two different thermal quenching processes characterized by two apparent activation energies, namely, 10.2 and 46.3 meV in the lower (100 to $\sim$200 K) and higher ($\sim$300 το $\sim$400 K) temperature regions, respectively.

We next investigate the PL decay dynamics in the corresponding time and temperature regions. Representative decay profiles in the $0-1$ μs time window are shown in Fig. 9. In the temperature regions from 77 to $\sim$325 K, the PL decay profiles
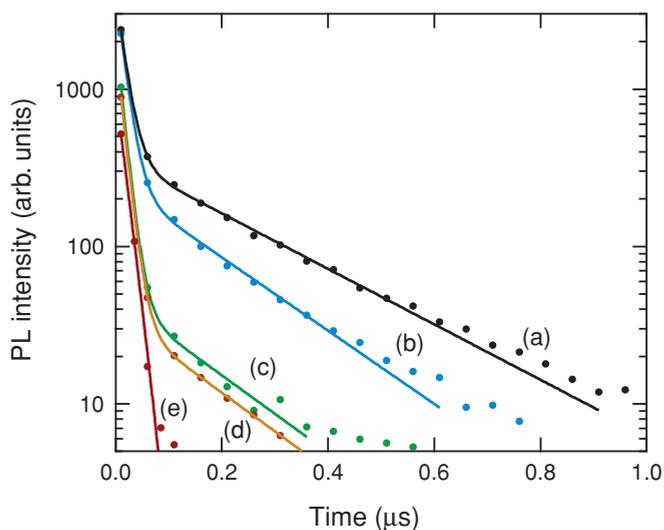
FIG. 9. (Color online) PL decay profiles at 395 nm in the $0-1$ μs time region measured at different temperatures: (a) 77, (b) 100, (c) 200, (d) 300, and (e) 400 K. Solid lines represent best fits of the data in (a)$-$(d) with a double-exponential function or those in (e) with a single-exponential function.
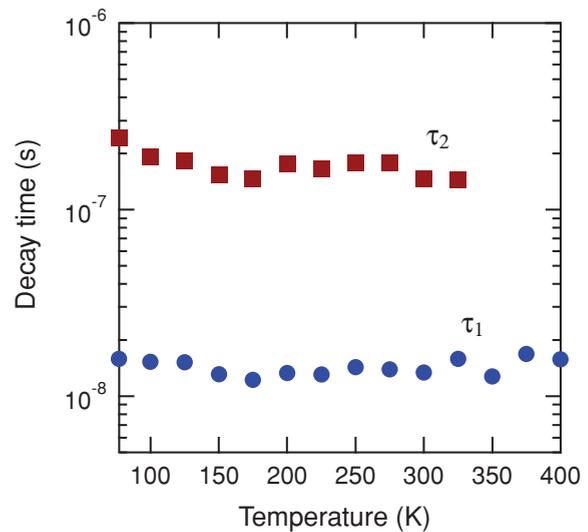
FIG. 10. (Color online) Temperature dependence of the fitted time constants, τ_1 and τ_2, obtained for the PL decay data shown in Fig. 9.

can be reasonably described by a double-exponential function characterized by fast (τ_1) and slow (τ_2) decay components,

$$I(t) = I_1 \exp(-t/\tau_1) + I_2 \exp(-t/\tau_2), \quad (3)$$

where $I(t)$ is the PL intensity at time t and I_i represents the initial intensity of the ith ($i = 1, 2$) component. The presence of the second decay component implies a feeding of the radiative transition from some trapping states. We should note, however, that the contribution of the slow decay component tends to decrease with increasing temperature and practically vanishes at temperatures higher than $\sim$350 K. The fitted values of the decay times (τ_1 and τ_2) are summarized in Fig. 10. The decay times of the fast and slow decay components are of the order of $\sim$10 and $\sim$100 ns, respectively, and both the decay times are almost constant within the fitting uncertainties over the entire temperature range investigated. This appears to be surprising since the emission intensity is observed to decrease with temperature, as shown in Fig. 8. We should note, however, that such PL characteristics, namely, the temperature-independent decay time and the temperature-dependent intensity, have often been reported for a defect-related emission in semiconductors and insulators where the intensity reduction stems from thermal activation of electrons out of the defect upper energy level into the conduction band.[28,29] As will be discussed in Sec. IV, this type of thermal activation of electrons is indeed likely to occur in the excitation process of the present MgO sample.

2. Microsecond-to-millisecond time scale

Figure 11 shows the temperature dependence of the time-integrated PL spectra of the deposited MgO powder in the 1 μs$-$25 ms time window under the same excitation condition presented above. The PL spectra in this time window are characterized not only by the F^+-center emission at $\sim$390 nm but also by the F-center emission at $\sim$500 nm, especially at high temperatures. Figure 12 shows the changes in the PL intensity at 395 and 500 nm with temperature. The PL intensity at 395 nm has two maxima at 125 and 325 K, whereas the PL
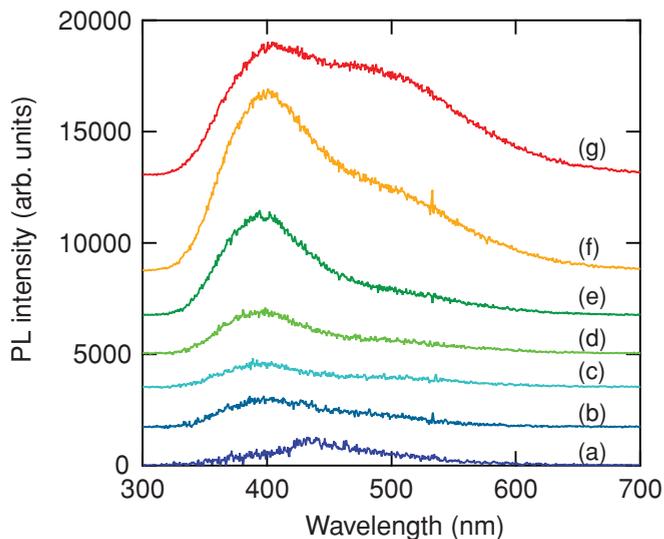
FIG. 11. (Color online) Time-integrated (1 μs−25 ms) PL spectra of the deposited MgO powder under excitation of the fourth harmonic (266 nm) of a pulsed Nd:YAG laser measured at different temperatures: (a) 77, (b) 125, (c) 225, (d) 250, (e) 275, (f) 350, and (g) 400 K.

intensity at 500 nm is almost null up to 225 K and shows a monotonic increase at temperatures higher than 250 K. The observed changes in the PL intensity with temperature strongly imply that the emission process in this time window is activated by some thermally induced events.

To get further knowledge about the expected thermally activated recombination processes, the PL decay was monitored at 395 nm in the time scale from 10^{-7} to 10^{-2} s at temperatures from 77 to 450 K (see Fig. 13). All the decay profiles are highly nonexponential, and some of them show a power-law dependence over more than 3−4 decades of time, yielding the fitted values of the exponent of 0.1−0.15. Furthermore, the temporal decay exhibits quite complicated temperature
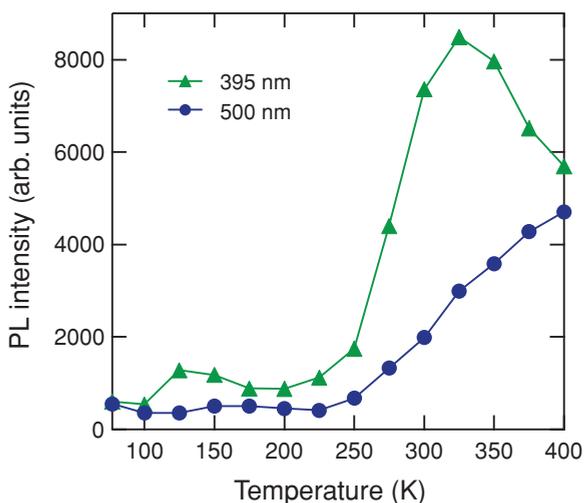
FIG. 12. (Color online) Temperature dependence of the PL intensities at 395 and 500 nm obtained for the time-integrated PL spectra shown in Fig. 11.
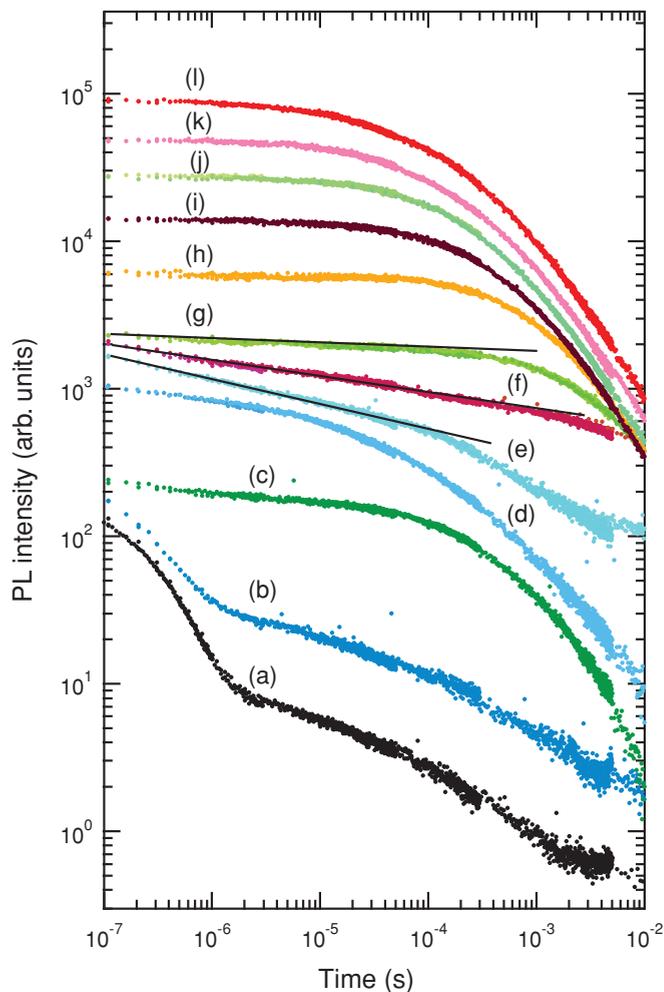
FIG. 13. (Color online) PL decay profiles at 395 nm in the time region from 10^{-7} to 10^{-2} s measured at different temperatures: (a) 77, (b) 100, (c) 150, (d) 200, (e) 250, (f) 275, (g) 300, (h) 325, (i) 350, (j) 375, (k) 400, and (l) 425 K. The curves are arbitrarily shifted along the y axis for clarity of presentation. Solid lines represent the results of fitting with a power-law function; the fitted values of the power-law exponent are 0.10, 0.15, and 0.12 for the data obtained at 200, 250, and 275 K, respectively.

dependence, in harmony with the anomalous temperature dependence of the PL intensity shown in Fig. 11.

As for the F-center PL band at ∼500 nm, we found that the PL signals decay more slowly, showing little or no signs of a decrease in intensity in this time window. The decay profiles of the F-center band will hence be shown below.

3. *Millisecond-to-second time scale*

Figure 14 shows the decay characteristics of the F-center emission at 500 nm in the 1 ms−10 s time window. In this time window we carried out the time-resolved PL measurements by using a monochromated xenon lamp (excitation wavelength $\lambda_{ex} = 256$ nm) and a mechanical shutter. Similar to the case of the PL decay curves of the F^+ center mentioned above, the F-center emission in this time window shows a highly nonexponential decay and complex temperature dependence. It appears that the decay curves consist of two components
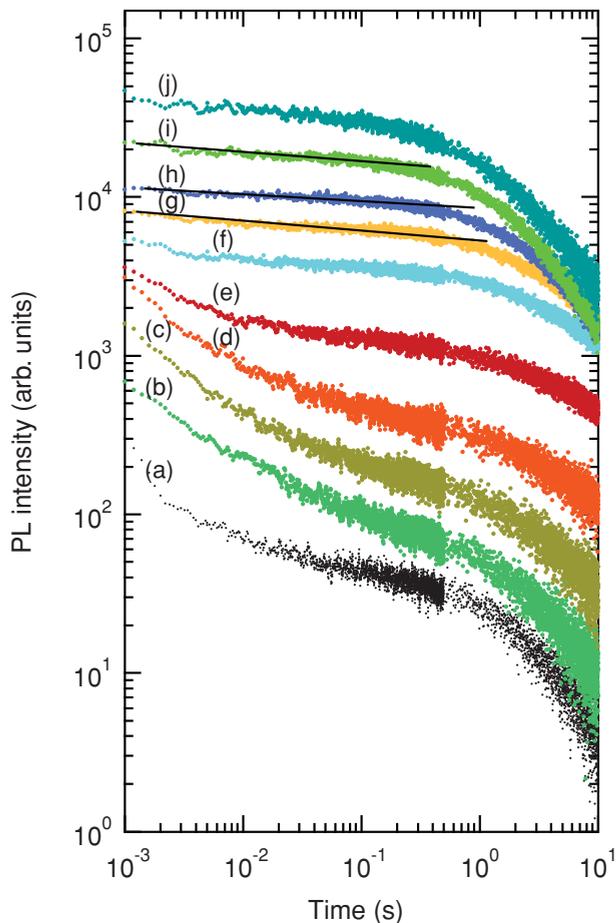
FIG. 14. (Color online) PL decay profiles at 500 nm in the time region from 10^{-3} to 10^1 s measured at different temperatures: (a) 77, (b) 125, (c) 175, (d) 200, (e) 225, (f) 250, (g) 275, (h) 300, (i) 325, and (j) 350 K. The curves are arbitrarily shifted along the y axis for clarity of presentation. Solid lines represent the results of fitting with a power-law function; the fitted values of the power-law exponent are 0.04, 0.04, and 0.05 for the data obtained at 275, 300, and 325 K, respectively.

especially for temperatures below ∼200 K: a fast component in the order of 1–2 ms and a slow component in the order of several seconds. The slow decay component tends to contribute more to the whole decay process with increasing temperature, showing a power-law-like decay for temperatures above ∼275 K.

It is also interesting to note that under continuous irradiation with 256-nm light the intensity of the F-center emission shows a gradual increase during the first couple of seconds of irradiation and then reaches a constant value (see Fig. 15). The observed PL transients were tentatively fitted with a double-exponential function,

$$I(t) = I_0 - I_3 \exp(-t/\tau_3) - I_4 \exp(-t/\tau_4), \qquad (4)$$

where I_0 is the constant PL intensity attained for a longer duration of irradiation time, and I_i and τ_i are the degree of transient increase in the PL intensity and the rise time of the ith ($i = 3, 4$) component, respectively. The fitted values of I_i and τ_i are summarized in Fig. 16. We should note that all these parameters exhibit a similar temperature dependence,
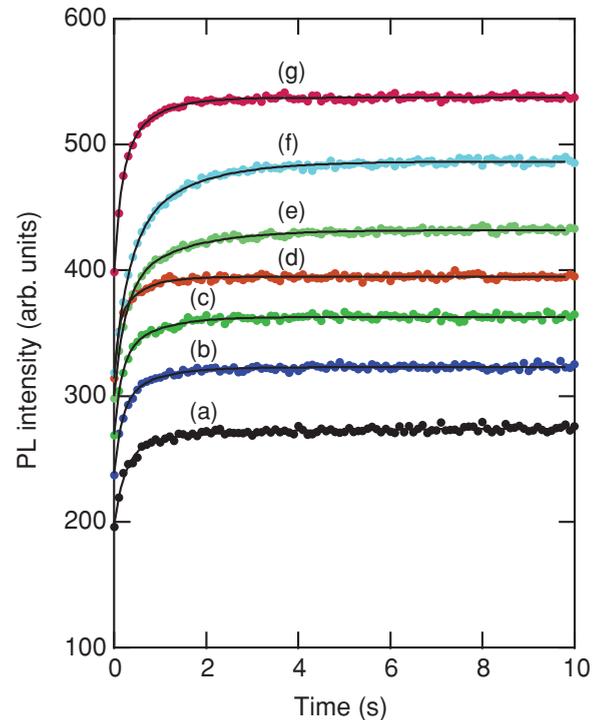
FIG. 15. (Color online) Transient PL increase at 500 nm during continuous excitation of 256-nm light measured at different temperatures: (a) 77, (b) 100, (c) 150, (d) 200, (e) 250, (f) 300, and (g) 350 K. The curves are arbitrarily shifted along the y axis for clarity of presentation. Solid lines represent best fits of the data with Eq. (4).

showing maxima at temperatures of 250−300 K. In general, PL rise is observed as a result of the capture and release of photoexcited carriers by localized traps during illumination, and the rise time represents the rate of carrier capture.[30] The observed temperature dependence of I_i and τ_i allows us to confirm that the relevant carrier filling and emptying processes are thermally activated. Note also that the observed rise time is slow (∼0.1−1 s), indicating a rather long capture time of the carriers in the emission process of the F center.

E. Effect of temperature on the lasing spectra

Detailed lasing characteristics of the present deposited MgO powder will be reported elsewhere.[31] In this paper, we concentrate our interest mainly on the temperature dependence of the PL spectra obtained below and above the threshold pump fluence for lasing (∼60 mJ/cm²), which is almost temperature invariant within experimental uncertainty.

Figure 17 shows the PL spectra of the MgO sample measured at 77 and 300 K under excitation of the fourth harmonic (266 nm) of a pulsed Nd:YAG laser with a gate width of 0.5 s. As far as the PL spectra below the lasing threshold are concerned, there are no apparent differences between the PL spectra measured at 77 and 300 K, both showing a broad band peaking at ∼390 nm. The spectral shapes shown in Fig. 17 are somewhat different from those obtained under continuous irradiation with a monochromated xenon lamp (see Fig. 4). The difference between the spectral shapes shown in Figs. 4 and 17 probably results from the difference in gate width used to obtain the respective spectra. The gate width (0.5 s) employed
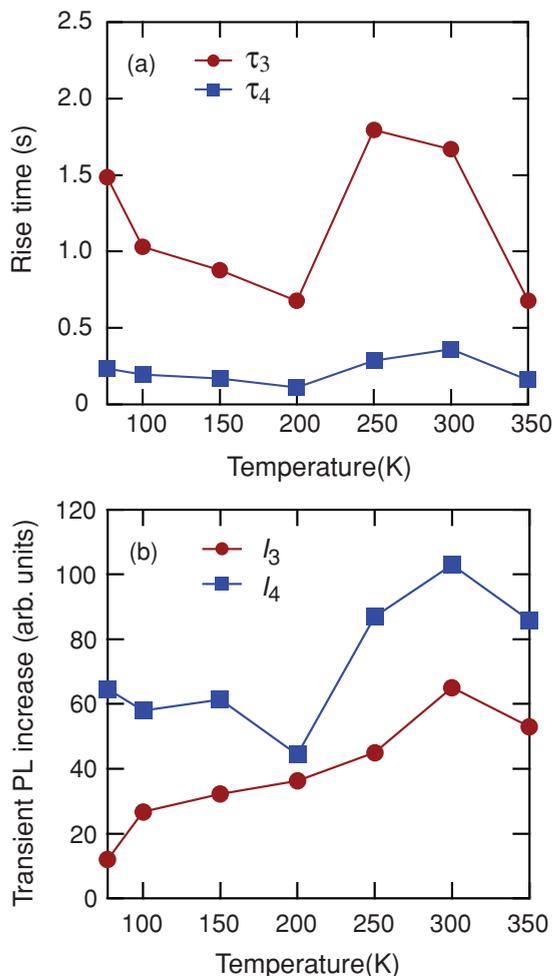
FIG. 16. (Color online) Results of fitting of the transient PL data shown in Fig. 15 with Eq. (4): (a) τ_3 and τ_4, (b) I_3 and I_4.

FIG. 17. (Color online) PL spectra of the MgO sample below and above the lasing threshold ($\sim$60 mJ/cm^2) measured at different temperatures: (a) 77 and (b) 300 K. The pumping fluence of the fourth harmonic (266 nm) of a pulsed Nd:YAG laser used to obtain each PL spectrum is shown. The asterisk indicates the second harmonic (532 nm) of the Nd:YAG laser contaminated in the incident beam.

in the pulsed laser experiments shown in Fig. 17 will not be long enough to detect all the photons associated with the longer-lived F-center emission.

Above the lasing threshold, spectral narrowing is observed irrespective of temperature. However, the spectrum obtained at 300 K is far broader than that obtained at 77 K, although the latter spectrum still retains a broad-band nature owing to the strong coupling between the electronic states of the emission centers and the crystal phonons. This result demonstrates that the thermal vibrations of the crystal lattice affect the stimulated emission process, hence showing the temperature dependence of linewidths in the lasing spectra.

IV. DISCUSSION

A. The F^+-center emission

1. Nanosecond-to-microsecond time scale

In this time region, the decay curves are well described by a double-exponential function characterized by fast (τ_1) and slow (τ_2) decay components (see Fig. 9). It is most likely that the fast component, which is of the order of $\lesssim$10 ns, will basically represent the intrinsic radiative decay time of the F^+ center. On the other hand, the slow component, which is of

FIG. 18. Schematic diagram of the ground (level 1), exited (level 2). and trapping (level 3) states associated with the intracenter transition of the F^+ center along with the parameters used to fit observed decay kinetics to a three-level model.
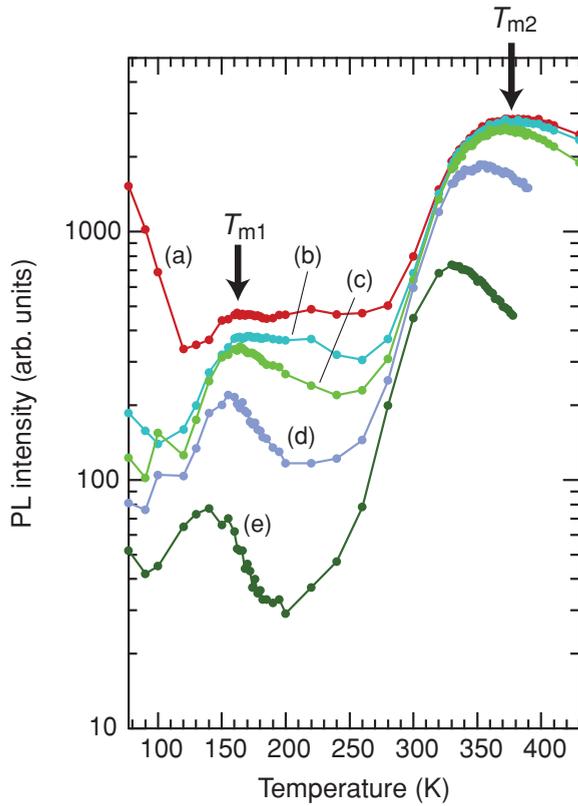
FIG. 19. (Color online) Transient thermoluminescence curves of the F^+ center emission at different sampling times t_s: (a) 10^{-7}, (b) 10^{-6}, (c) 10^{-5}, (d) 10^{-4}, and (e) 10^{-3} s. These curves are constructed from the PL decay profiles shown in Fig. 13.

the order of $\sim$100 ns, presumably results from the trapping of the photoexcited carriers during the excitation event of the F^+ center. This can be rationalized by considering the following kinetic scheme.

Phenomenologically, the observed double-exponential decay kinetics can be interpreted in terms of a three-level system with the following rate equations describing time-dependent population changes for the respective energy levels (see Fig. 18),

$$\frac{dN_1}{dt} = p_{21}N_2 + p_{31}N_3, \tag{5}$$

$$\frac{dN_2}{dt} = -(p_{21} + p_{23})N_2 + p_{32}N_3, \tag{6}$$

$$\frac{dN_3}{dt} = p_{23}N_2 - (p_{32} + p_{31})N_3, \tag{7}$$

with

$$N_1 + N_2 + N_3 = N_0, \tag{8}$$

where N_i is the population in the ith state, p_{ij} is the transition probability per unit time from the ith level to the jth level, and N_0 is the total number of populations in the system. In the present case, levels 1 and 2 correspond to the ground and the excited states of the F^+ center, and level 3 represents the trap state. The solution for this set of coupled linear differential

equations yields a double-exponential decay function for $N_2(t)$:[32]

$$N_2(t) = A_1 \exp(-t/\tau_1) + A_2 \exp(-t/\tau_2), \tag{9}$$

with A_1 and A_2 being constants which are determined by initial conditions of the system, and τ_1 and τ_2 ($\tau_1 < \tau_2$) are the roots of the coefficient matrix given by Eqs. (6) and (7),

$$\tau_{1,2}^{-1} = \tfrac{1}{2}(p_{21} + p_{23} + p_{32} + p_{31})$$
$$\mp \tfrac{1}{2}[(p_{21} + p_{23} + p_{32} + p_{31})^2$$
$$- 4(p_{32}p_{21} + p_{23}p_{31} + p_{21}p_{31})]^{1/2}. \tag{10}$$

We here assume that the radiative transition rate of the F^+ center (p_{21}) is much greater than the transition rates related to the trap state, namely, $p_{21} \gg p_{23}, p_{32}, p_{31}$. Under this assumption, we obtain

$$\tau_1^{-1} \approx p_{21}, \tag{11}$$

$$\tau_2^{-1} \approx p_{32} + p_{31}. \tag{12}$$
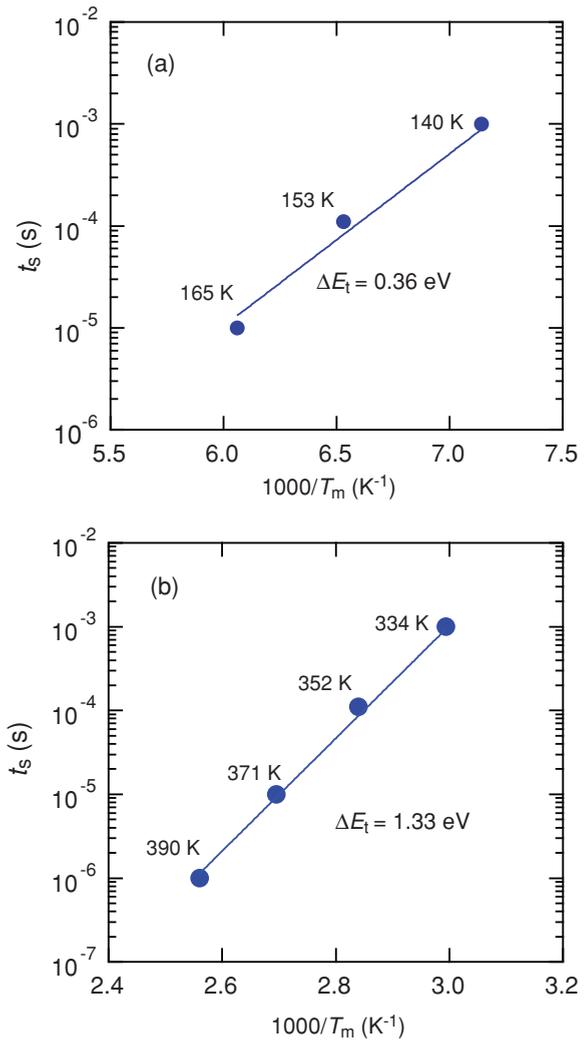
FIG. 20. (Color online) Log-linear plot of t_s as a function of $1/T_m$, representing the shift of the peak position at (a) $\sim$140$-$160 and (b) $\sim$330$-$390 K in Fig. 19.

It hence follows that the fast (τ_1) and slow (τ_2) decay times represent the radiative decay time of the F^+ center and the carrier capture time of the trap state, respectively, as expected earlier.

We should note, however, that the real excitation process will not be as simple as expected from the above three-level scheme. This is because, as mentioned in Sec. III D 1, the PL process in this time domain is characterized by the temperature-dependent intensity and the temperature-independent decay time, implying the thermalization process of electrons from the excited level to the conduction band. This type of emission has been demonstrated to occur when the relevant energy levels of the system are characterized by a close proximity of the excited level with the bottom of the conduction band and by a large energy separation between the excited level and the emission level.[28,29] A more detailed emission scheme will be discussed again in Sec. IV A 3.

2. Microsecond-to-millisecond time scale

The increase in the PL intensity with temperature in this time region (see Fig. 12) implies a thermally activated emission mechanism analogous to the one called thermoluminescence (TL). If thermal activation from traps plays a vital role in the decay kinetics in the μs-to-ms time window, a transient thermoluminescence (TTL) curve, which represents the temperature dependence of the emission intensity at a certain delay time after excitation, exhibits a peak maximum at a certain temperature.[33,34] Figure 19 shows a series of TTL curves constructed from the PL decay profiles shown in Fig. 13 at different delay times. One sees from Fig. 19 that the constructed TTL curves are characterized by two maxima at temperatures at $\sim$140–160 K (T_{m1}) and $\sim$330−390 K (T_{m2}). The appearance of maxima in the TTL curves corroborates that the thermally activated emission is the major emission process in this time region.

Previously, TLL curves were kinetically analyzed, and the following relationship was found to exist:[33]

$$t_s \propto \exp(\Delta E_t / k_B T_m), \qquad (13)$$

where t_s is the sampling time or delay time, ΔE_t the thermal activation energy of the trapped carriers, T_m the maximum temperature in TTL curves, and k_B the Boltzmann constant. According to Eq. (13), the plot of $\ln(t_s)$ vs $1/T_m$ gives a straight line, whose slope yields the value of ΔE_t. Figure 20 shows the semilog plot between t_s and $1/T_m$ obtained for the two peak maxima at T_{m1} and T_{m2}, yielding the values of $\Delta E_t = 0.36$ and 1.33 eV, respectively. The above arguments clearly demonstrate that, as for the F^+ center, there exist two types of thermally stimulated emission processes with different activation energies in the μs-to-ms time window.
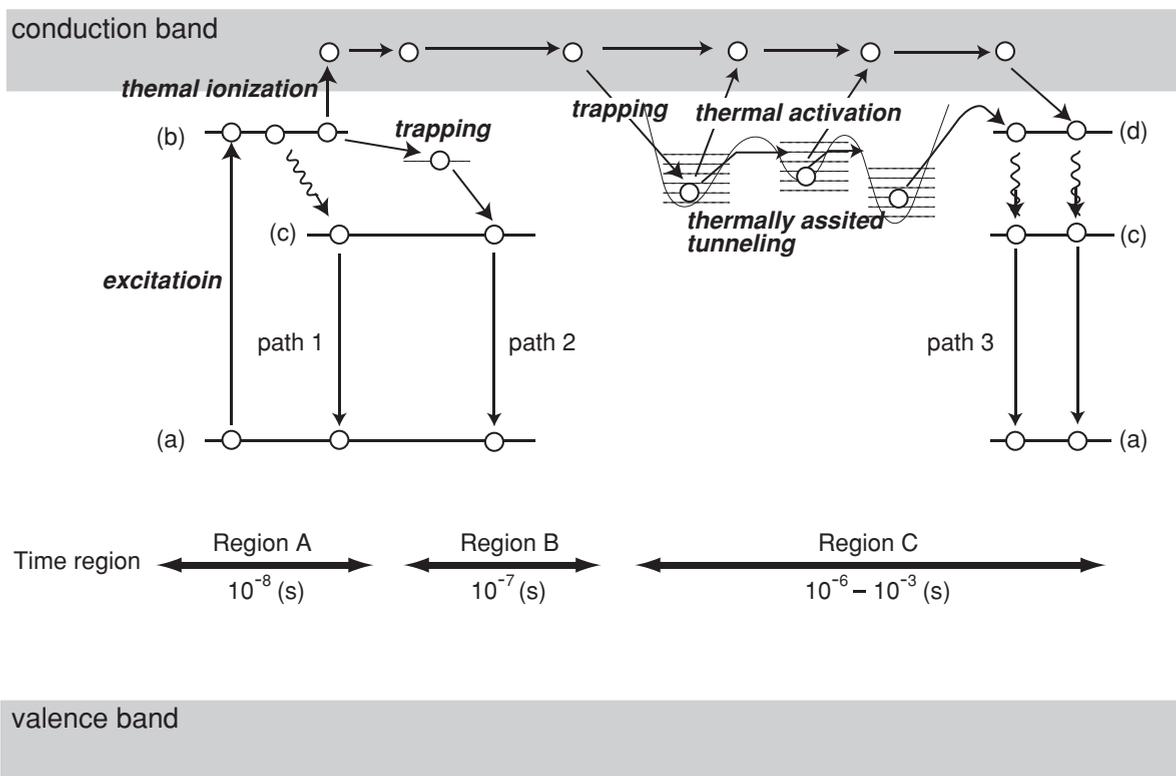
FIG. 21. A model of the excitation, trapping, and recombination processes associated with the F^+ center, which proceeds from the left-hand side to the right-hand side in the diagram: (a) the ground-state level, (b) the excited-state level, (c) the emission-state level, and (d) the excited-state level formed by the recombination between the F^{2+} center and a free electron in the conduction band [Eq. (18)]. The dashed lines represent possible trapping states.

3. Mechanism of radiative recombination

Considering the discussion given above, we can propose a model of the whole excitation, trapping, and recombination processes of the F^+ center (see Fig. 21). When the F^+ center absorbs ~250 nm photons, the resulting photoexcited electrons will return to the ground state via at least three types of radiative paths, namely, (1) direct radiative recombination without trapping (see path 1 in Fig. 21), (2) indirect radiative recombination via trapping without ionization (see path 2 in Fig. 21), and (3) indirect radiative recombination via trapping initiated by ionization (see path 3 in Fig. 21).

Path 1 is likely to contribute to the exponential decay with a decay time of ~10 ns [τ_1 in Eq. (3) and see region A in Fig. 21], which will basically represent the radiative lifetime of the following intracenter transition,

$$F^+ + h\nu(250 \text{ nm}) \rightarrow F^{+*}(\text{excited state}), \qquad (14)$$

$$F^{+*} \rightarrow F^+ + h\nu(360 \text{ nm}). \qquad (15)$$
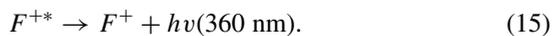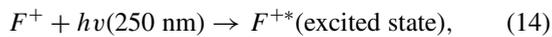
Path 2 is as an alternative path of the intracenter transition; however, the path is characterized by trapping, which contributes to the decay dynamics on a time scale of several hundreds of nanoseconds [τ_2 in Eq. (3) and see region B in Fig. 21]. As mentioned in Sec. IV A 1, these two intracenter recombination processes can be more simply represented by the three-level scheme shown in Fig. 18.

Path 3, which will play a vital part in the decay dynamics in the μs-to-ms time scale (see region C in Fig. 21), is initiated by the thermally induced photoionization of the F^+ center, forming an F^{2+} center (bare oxygen vacancy) and the electron in the conduction band,

$$F^+ + h\nu(250 \text{ nm}) \rightarrow F^{+*}, \qquad (16)$$

$$F^{+*} + kT \rightarrow F^{2+} + e^-. \qquad (17)$$
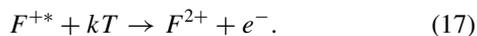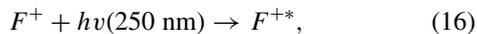
The concept of F^+ photoionization by electron release has been proposed previously to explain its delayed PL characteristics.[27] The activation energy for the above thermalization process must be substantially smaller than that of other possible competing nonradiative recombination processes, otherwise the electron in the F^{+*} state will recombine through a radiative or a nonradiative channel immediately. Consistent with the proposed scheme, the PL emission just after the excitation or in the ns-to-μs time region is characterized by two different thermal quenching processes with two apparent activation energies of 10.2 and 46.3 meV (see Fig. 8). We believe that the lower and higher activation energy processes correspond to the thermally induced photoionization of the F^+ center and the normal nonradiative recombination, respectively.

Once liberated into the conduction band, the electron will exhibit carrier transport via thermally induced trapping and releasing processes. It is interesting to note that in the μs-to-ms time window, PL signals decay in a power-law manner (see Fig. 13), namely, $I(t) \propto t^{-\gamma}$, which often arises from thermal excitation of electrons from traps when there is a distribution in the energy levels of traps.[35] We should note, however, that the γ values obtained here are rather small ($\gamma \simeq 0.04-0.15$) as
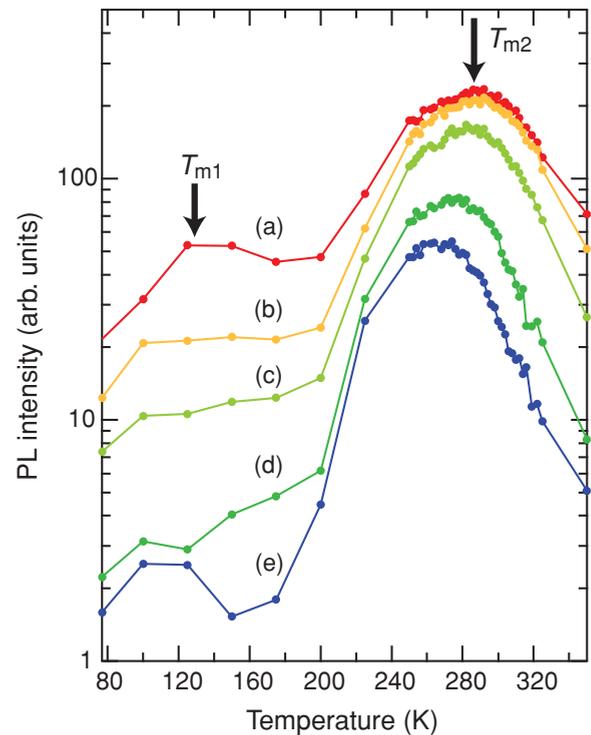
FIG. 22. (Color online) Transient thermoluminescence curves of the F center emission at different sampling times t_s: (a) 10^{-2}, (b) 10^{-1}, (c) 1, (d) 5.0, and (e) 10 s. These curves are constructed from the PL decay profiles shown in Fig. 14.

compared with the value ($\gamma = 0.95-1.5$) observed commonly in solids.[35] Such a low value of γ was reported and discussed previously although only in a few papers,[36–38] demonstrating that γ much lower than 1 results from thermally assisted tunneling motion of trapped carriers. The tunneling mechanism is in principle a temperature-independent process. It is, however, possible that tunneling is thermally assisted; that is, the trapped charge is first thermally raised to a certain energy level over the ground-state level and then tunnels through a barrier.[39]
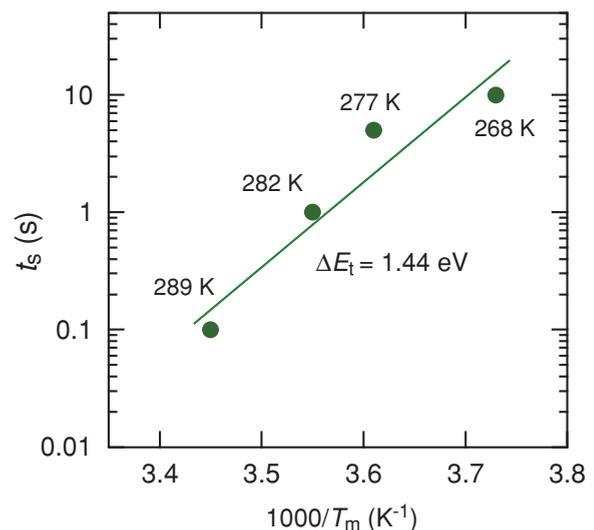
FIG. 23. (Color online) Log-linear plot of t_s as a function of $1/T_m$, representing the shift of the peak position at ~270−290 K in Fig. 22.

Thus, we propose that the carrier transport occurring in path 3 results not only from thermal activation of trapped electrons into the conduction band but also from the thermally assisted tunneling between adjacent trapping centers.

After these series of transport evens, the electron will eventually recombine with the originally distant F^{2+} center, giving rise to a delayed F^+-center emission as follows:

$$F^{2+} + e^- \rightarrow F^{+*}, \tag{18}$$

$$F^{+*} \rightarrow F^+ + hv(360 \text{ nm}). \tag{19}$$

Thus, the recombination process in path 3 is, in principle, an intercenter recombination or a bimolecular-type recombination, where independently generated F^{2+} centers and electrons recombine.

B. The *F*-center emission

Similar to the TTL curves obtained for the F^+-center emission, the TTL curves constructed from the PL decay profiles of the F center exhibit two maxima at $\sim$120–160 and $\sim$300−370 K (see Fig. 22). We estimated the thermal activation energy ΔE_t only for the high-temperature maxima in Fig. 22 since the exact peak position of the low-temperature maxima was not clear. From the plot of $\ln(t_s)$ vs $1/T_m$ (see Fig. 23), ΔE_t was estimated to be 1.44 eV, which is very similar to the one obtained for the high-temperature maxima of the F^+ center (1.33 eV). This strongly suggests that the underlying thermally activated processes of the trapped electrons are very similar between the F and F^+ centers.

Figure 24 illustrates a possible emission mechanism of the F center. The emission scheme shown in Fig. 24 is apparently similar to that proposed for the F^+ center shown in Fig. 21. However, there is a decisive difference between the emission processes of the F and F^+ centers. That is, the intracenter emissions, which correspond to paths 1 and 2 in Fig. 21, are unlikely in the emission process of the F center since we hardly observe the F center emission in the ns-to-μs time region, although it is spin allowed.[17] This indicates that, as has often been assumed,[17,19] most of the excited F centers are ionized by electron release to the conduction band because of a negligibly small thermal activation energy. Thus, the excitation and ionization processes of the F center are described as follows:

$$F + hv(250 \text{ nm}) \rightarrow F^*, \tag{20}$$

$$F^* + kT \rightarrow F^+ + e^- kT \approx 0 \text{ eV}. \tag{21}$$
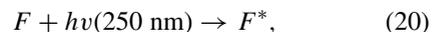
The above consideration also implies that the F^+ center will behave as a very shallow trap. This is because, even if the excited state of the F center (F^*) is created as a result of the reverse reaction of ionization, namely,

$$F^+ + e^- \rightarrow F^*, \tag{22}$$

the loosely bound electron in the F^* center will be excited into the conduction band again [see Eq. (21)], resulting in reionization. We hence consider that a rather long capture time ($\sim$0.1−1 s) of the carriers deduced from the PL transient shown in Fig. 15 results from a prolonged transport period associated with the above reionization process before the
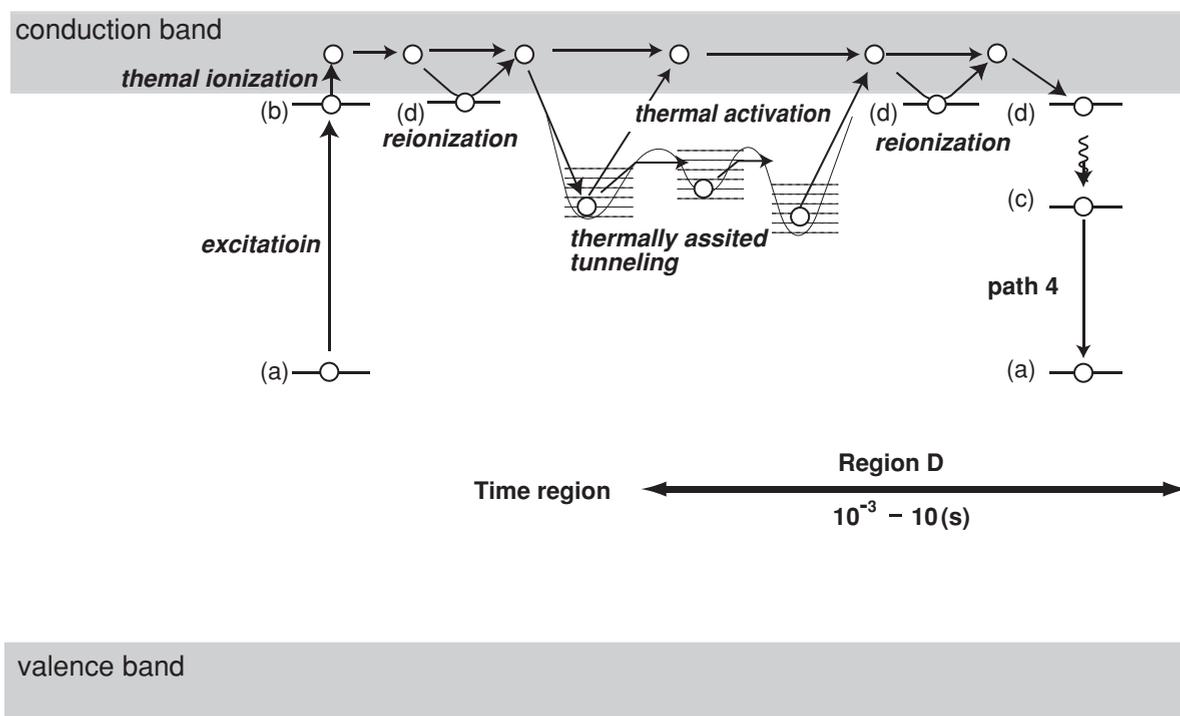
FIG. 24. A model of the excitation, trapping, and recombination processes associated with the F center, which proceeds from the left-hand side to the right-hand side in the diagram: (a) the ground-state level, (b) the excited-state level, (c) the emission-state level, and (d) the excited-state level formed by the recombination between the F^+ center and a free electron in the conduction band [Eq. (22)]. The dashed lines represent possible trapping states.

radiative recombination event finally occurs (see path 3 in Fig. 24).

C. Origin of trap centers

Thus we have shown that the present F- and F^+-center emissions can be reasonably interpreted in terms of trap-related emission mechanisms. However, one important question still remains unanswered: What is the origin of electron trapping centers?

In previous studies,[17,18] the dominant electron trap controlling the F- and F^+-center emissions in MgO has been identified as the H^- center, which can convert to the H^{2-} center by trapping an electron. The thermal release of an electron from the H^{2-} center was observed as a thermoluminescence peak near 260 K, characterized by an activation energy of 0.56 eV.[40] It has been demonstrated also that the successive electron capture by the H^- center leads to an extremely long emission lifetime, which can last as long as 10^3 s.[17,18]

In the present MgO sample, however, the concentration of the H^- center is negligibly low, and the observed trap-related PL phenomena are quite different from those reported previously. Thus, other types of trap centers need to be considered to understand the present PL characteristics.

One of the probable candidates is the F^+ center, which will act as a very shallow trap, as mentioned above. In addition to this positively charged single-vacancy center, we propose that positively charged anion vacancy pairs, such as F_2^+ and F_2^{2+} centers, are likely candidates for electron trapping centers as well. Since the excited states of aggregated oxygen vacancies generally lie at lower energies than those of single oxygen vacancies,[41] the F_2^+ and F_2^{2+} centers will be able to behave as deep electron traps.

It has been demonstrated that MgO crystals containing a large amount ($\gtrsim 10^{18}$ cm^{-3}) of single anion vacancies exhibit several absorption bands attributed to anion vacancy pairs in the wavelength region from $\sim$320 to $\sim$400 nm, showing luminescence bands at 375 (F_2 centers), 441 (F_2^{2+} centers), and 475 nm (F_2^+ centers).[42,43] To confirm whether or not these aggregate vacancies exist in the present MgO sample, we measured the PL spectrum under excitation of the third harmonic (355 nm) of a pulsed Nd:YAG laser. A typical example of the emission spectra is shown in Fig. 25. One sees from Fig. 25 that the observed spectrum has three emission bands located at $\sim$380, $\sim$435, and $\sim$475 nm, which are in reasonable agreement with the reported emission wavelengths of the F_2, F_2^{2+}, and F_2^+ centers, respectively. It is hence probable that these anion vacancy pairs are present in the present sample and also that some of these vacancies, especially in the form of positively charged ones, are responsible for a series of trapping and thermally activated detrapping events.

The formation of anion vacancy pairs further implies that some of the single-vacancy centers are not completely isolated but are closely located to each other, forming weakly coupled F-type center pairs, e.g., $F + F$, $F^+ + F$, and $F^+ + F^+$ pairs. We suggest that these weakly coupled pairs are responsible for the electron tunneling inferred from the PL decay measurements shown in Figs. 13 and 14. A similar tunneling assisted excitation process between F and F^+ center pairs was previously proposed by Edel et al.[44] to account for the
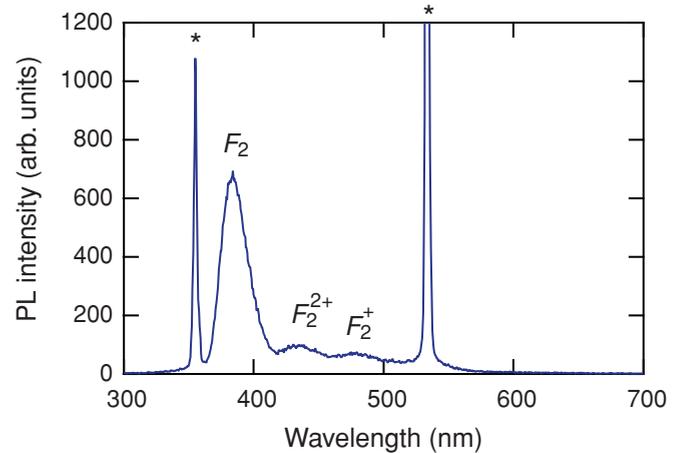
FIG. 25. (Color online) PL spectrum of the deposited MgO powder under excitation of the third harmonic (355 nm) of a pulsed Nd:YAG laser measured at room temperature. The two sharp lines indicated by the asterisk result from the third (355 nm) and second (532 nm) harmonic of a pulsed Nd:YAG laser involved in the incident laser beam.

long-lived components of the F-center emission in additively colored MgO crystals.

In addition to these F- and F_2-type centers, it is probable that other unidentified defects located at the surface and/or in the bulk are responsible for the electron trapping events. Further works need to be carried out to definitely identify the trapping centers contributing to the observed PL phenomena.

D. Effect of lattice vibrations on the lasing characteristics

In Sec. III E, we have shown that the PL spectra above lasing threshold exhibit temperature-dependent broadening. In our previous paper,[6] we have proposed that the lasing feature at 384 nm can be attributed not only to the F^+-center emission but also to the $3d\,^3D \rightarrow 3p\,^3P$ transition in excited neutral Mg (Mg$^\circ$), indicating that both the F^+ center and the Mg$^\circ$ line emissions are responsible for random lasing.[45] The Mg atomic emission is expected to be initiated by the following photoinduced charge exchange between the F-type center and an Mg^{2+} ion in the crystalline lattice,[6,46]

$$F^+(\text{or } F) + \text{Mg}^{2+} + h\nu(250 \text{ nm}) \rightarrow F^{2+}(\text{or } F^+) + \text{Mg}^+.$$

(23)
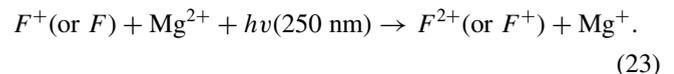
Under low-fluence excitation, the reverse reaction of Eq. (19) will occur nonradiatively, showing no Mg-related atomic emissions. Under high-fluence excitation, however, a large number of photoexcited electrons are supposed to exist in the conduction band according to the thermally induced ionization of the F and F^+ centers [see Eqs. (17) and (21)]. This will lead to the following radiative recombination between the Mg$^+$ ion and the photoexcited electron,[6]

$$\text{Mg}^+ + e^- \rightarrow \text{Mg}^{\circ *}, \quad (24)$$

$$\text{Mg}^{\circ *} \rightarrow \text{Mg}^\circ + h\nu'(384 \text{ nm}). \quad (25)$$
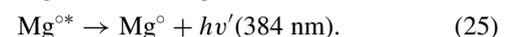
The above scheme implies that the Mg$^\circ$ line emission and the random lasing are in principle different phenomena.

However, it is reasonable to expect that the former atomic emission is amplified once the lasing condition for the F^+-center emission is reached because the energy of the Mg° line emission resides within the broad spectral range of the F^+-center emission. The temperature-dependent broadening of the lasing spectra also suggests that the F^+-center emission and the Mg° line emission do not occur independently, but rather these two types of emissions are strongly correlated to each other via lattice vibrations. In other words, the lattice vibrations are coupled not only to the electronic states of the F^+ center but also to those of Mg°, giving rise to a thermally broadened lasing spectrum with a peak at 384 nm.

It is hence probable that the Mg^+ and Mg° are bound in the crystalline lattice during the whole photoexcitation and stimulated emission processes. This consideration corroborates that the Mg° atomic emissions do not result from plasma plume, which is produced off the surface of the specimen by focusing a high-power laser. Previous laser-produced plasma measurements on a MgO single crystal have demonstrated that the onset fluence for plume-related Mg° emissions is $\sim$ 2 J/cm^3 per pulse,[47] which is far above the lasing threshold of the present MgO sample ($\sim$60 mJ/cm^2).

Finally, it is interesting to mention that the decay time of the present lasing signals is 20 ns,[5] which is too fast for the thermally excited electrons to be involved in the lasing event. This can explain the reason why the F^+-center emission is solely amplified because, as shown in Fig. 24, the F-center emission arises mostly from the delayed recombination of thermally excited electrons. We should note, however, that the Mg° line emission will not occur unless the F-type centers are thermally ionized to yield electrons in the conduction band.

V. SUMMARY AND CONCLUSIONS

From detailed time-resolved and temperature-dependent PL measurements on the MgO powder prepared by the solid phase reaction between Mg and B_2O_3, we can conclude the following

concerning the photoexcitation, trapping, and recombination processes of the F-type centers.

(1) Upon excitation of the F^+ center, the photoexcited electrons return to the ground state via three different paths, depicted in Fig. 21 as paths 1, 2, and 3. Paths 1 and 2 are responsible for the emission in the nanosecond-to-microsecond time scale and show a simple decrease in intensity with increasing temperature. On the other hand, the emission associated with path 3 is initiated by the thermally induced ionization of the F^+ center and is thermally activated, showing the delayed thermally stimulated luminescence in the microsecond-to-millisecond time scale.

(2) The emission scheme of the F center is similar to that of the F^+ center. In contrast to the case of the F^+ center, however, the photoexcitation of the F center results almost exclusively in the thermally induced ionization, leading only to the delayed PL signals in the millisecond-to-second time scale (path 4 in Fig. 24).

(3) The positively charged F- and F_2-type centers, such as the F^+, F_2^+, and F_2^{2+} centers, are likely candidates for the trapping centers, whereas weakly coupled F-type center pairs, e.g., $F + F$, $F^+ + F$, and $F^+ + F^+$ pairs, may contribute to the thermally assisted tunneling process.

(4) The temperature-dependent broadening of the lasing spectra implies that the F^+-center emission and the Mg° line emission at 384 nm are strongly correlated to each other via lattice vibrations.

(5) Delayed emission processes initiated by the thermally induced ionization of the F and F^+ centers will not contribute to the lasing scheme. However, the thermally induced ionization and the resulting free electrons in the conduction band are definitely required to induce the Mg° line emission, according to Eqs. (24) and (25).

Thus, we can conclude that the present colored MgO microcrystals are quite intriguing in that thermal excitations and lattice vibrations, which are normally unfavorable in terms of nonradiative recombination processes, play a variety of positive roles in showing the efficient PL emissions and the related lasing phenomena.

[1] B. Henderson and G. F. Imbusch, *Optical Spectroscopy of Inorganic Solids* (Oxford University Press, Oxford, 1989).

[2] K. J. Caulfield, R. Cooper, and J. F. Boas, J. Chem. Phys. **92**, 6441 (1990).

[3] W. C. Las and T. G. Stoebe, Radiat. Prot. Dosim. **8**, 45 (1984).

[4] M. A. Monge, A. I. Popov, C. Ballesteros, R. González, Y. Chen, and E. A. Kotomin, Phys. Rev. B **62**, 9299 (2000).

[5] T. Uchino and D. Okutsu, Phys. Rev. Lett. **101**, 117401 (2008).

[6] T. Uchino, D. Okutsu, R. Katayama, and S. Sawai, Phys. Rev. B **79**, 165107 (2009).

[7] J. Hu, Z. Zhang, M. Zhao, H. Qin, M. Jiang, Appl. Phys. Lett. **93**, 192503 (2009).

[8] A. Droghetti, C. D. Pemmaraju, and S. Sanvito, Phys. Rev. B **81**, 092403 (2010).

[9] C. Martínez-Boubeta, J. I. Beltrán, Ll. Balcells, Z. Konstantinovic, S. Valencia, D. Schmitz, J. Arbiol, S. Estrade, J. Cornil, and B. Martínez, Phys. Rev. B **82**, 024405 (2010).

[10] Y. Motoyama, H. Matsuzaki, and H. Murakami, IEEE Trans. Electron Devices **48**, 1568 (2001).

[11] Y. T. Matulevich, T. J. Vink, and P. A. Zeijlmans van Emmichoven, Phys. Rev. Lett. **89**, 167601 (2002).

[12] Y. H. Cheng, H. Kupfer, and F. Richter, J. Appl. Phys. **94**, 3624 (2003).

[13] T. Okada, T. Naoi, T. Yoshioka, J. Appl. Phys. **105**, 113304 (2009).

[14] S. Ho, S. Nobuki, N. Uemura, S. Mori, T. Miyake, K. Suzuki, Y. Mikami, M. Shiiki, and S. Kubo, J. Appl. Phys. **106**, 014911 (2009).

[15] Y. Chen, R. T. Williams, and W. A. Sibley, Phys. Rev. **182**, 960 (1969).

[16] L. A. Kappers, R. L. Kroes, and E. B. Hensley, Phys. Rev. B **1**, 4151 (1970).

[17] G. P. Summers, T. M. Wilson, B. T. Jeffries, H. T. Tohver, Y. Chen, and M. M. Abraham, Phys. Rev. B **27**, 1283 (1983).

[18] Y. Chen, R. Gonzalez, O. E. Schow, and G. P. Summers, Phys. Rev. B **27**, 1276 (1983).

[19] R. González, M. A. Monge, J. E. Munoz Santiuste, R. Pareja, Y. Chen, E. Kotomin, M. M. Kuklja, and A. Popov, Phys. Rev. B **59**, 4786 (1999).

[20] B. T. Jeffries, R. Gonzalez, Y. Chen, and G. P. Summers, Phys. Rev. B **25**, 2077 (1982).

[21] A. I. Popov, M. A. Monge, R. González, Y. Chen, and E. A. Kotomin, Solid State Commun. **118**, 163 (2001).

[22] H. Cao, Y. G. Zhao, S. T. Ho, E. W. Seelig, Q. H. Wang, R. P. H. Chang, Phys. Rev. Lett. **82**, 2278 (1999).

[23] D. S. Wiersma, Nat. Phys. **4**, 359 (2008).

[24] V. Sundaram, K. V. Logan, and R. F. Speyer, J. Mat. Res. **12**, 2657 (1997).

[25] W. Weimin, F. Zhengyi, W. Hao, and Y. Runzhang, J. Mat. Process. Technol. **128**, 162 (2002).

[26] R. González, Y. Chen, and M. Mostoller, Phys. Rev. B **24**, 6862 (1981).

[27] G. H. Rosenblatt, M. W. Rowe, G. P. Williams Jr., and R. T. Williams, Y. Chen, Phys. Rev. B **39**, 10309 (1989).

[28] T. Sauncy, C. P. Palsule, M. Holtz, S. Gangopadhyay, and S. Massie, Phys. Rev. B **53**, 1900 (1996).

[29] N. Sagawa and T. Uchino, Appl. Phys. Lett. **87**, 251923 (2005).

[30] K. W. Sun, A. Kechiantz, B. C. Lee, and C. P. Lee, Appl. Phys. Lett. **88**, 163117 (2006).

[31] Y. Uenaka and T. Uchino (unpublished).

[32] Q. Song, P. W. Bohn, G. J. Blanchard, J. Phys. Chem. B **101**, 8865 (1997).

[33] E. Nakazawa, Jpn. J. Appl. Phys. **23**, L755 (1984).

[34] J. Rennie, E. Nakazawa, and T. Koda, Jpn. J. Appl. Phys. **29**, 509 (1990).

[35] A. K. Jonscher and A. de Polignac, J. Phys. C **17**, 6493 (1984).

[36] M. Yamaga, Y. Masui, S. Sakuta, N. Kodama, and K. Kaminaga, Phys. Rev. B **71**, 205102 (2005).

[37] D. J. Huntley, J. Phys. Condens. Matter **18**, 1359 (2006).

[38] J. Trojan-Piegza, E. Zych, J. Hölsä, and J. Niittykoski, J. Phys. Chem. C **113**, 20493 (2009).

[39] J. Repp, G. Meyer, K.-H. Rieder, and P. Hyldgaard, Phys. Rev. Lett. **91**, 206102 (2003).

[40] G. P. Summers, B. T. Jeffries, R. Gonzalez and Y. Chen, Bull. Am. Phys. Soc. **27**, 413 (1982).

[41] B. D. Evans, G. J. Pogatshnik, and Y. Chen, Nucl. Instrum. Methods B **91**, 258 (1994).

[42] D. O. O'Connell, B. Henderson, and J. M. Bolton, Solid State Commun. **38**, 283 (1981).

[43] J. M. Bolton, B. Henderson, and D. O. O'Connell, Solid State Commun. **38**, 287 (1981).

[44] P. Edel, B. Henderson, and R. Romestain, J. Phys. C **15**, 1569 (1982).

[45] Additional peaks at 448 and 518 nm can be attributed to the $4f \rightarrow 3d$ transition of Mg^+ and the $4s \rightarrow 3p$ transition of Mg°, respectively.

[46] J. T. Dickinson, S. C. Langford, J. J. Shin, and D. L. Doering, Phys. Rev. Lett. **73**, 2630 (1994).

[47] D. R. Ermer, S. C. Langford, and J. T. Dickinson, J. Appl. Phys. **81**, 1495 (1997).